ANALYSIS AND MODELING OF SUMMERTIME CONVECTIVE CLOUD AND PRECIPITATION STRUCTURE OVER THE SOUTHEASTERN UNITED STATES

Semiannual report for the period 15 March to 15 September 1988

NASA Grant NAG8-654

Kevin R. Knupp

Atmospheric Science and Remote Sensing Lab

Johnson Research Center

University of Alabama in Huntsville

Huntsville, AL 35899

1. Introduction

This report describes work performed under NASA Grant NAG8-654 for the period 15 March to 15 September 1988. This work entails primarily data analysis and numerical modeling efforts that are related to the 1986 Satellite Precipitation and Cloud Experiment (SPACE). In the following, the SPACE acronym is used along with the acronym COHMEX, which represents the encompassing Cooperative Huntsville Meteorological Experiment. Progress made during the second half of this first year effort has included:

1) installation and testing of the the RAMS numerical modeling system on the Alabama CRAY X-MP/24;
2) a start on the analysis of the mesoscale convective system (MCS) of 13 July 1986 COHMEX case;
3) a cursory examination of a small MCS that formed over the COHMEX region on 15 July 1986.

Details under each of these individual tasks are given in the following sections.

2. RAMS Installation

During the latter half of May, 1988, Mr. Craig Tremback of Colorado State University installed and tested the Regional Atmospheric Modeling System (RAMS) on the State of Alabama CRAY X-MP/24 computer. This system is device dependent in that jobs may be submitted from the local VAX 11/785 minicomputer (operating under the VMS environment) in batch mode to the CRAY, via a high-speed T1 link (1.5 Mb/sec). Likewise, RAMS output can be transferred to the local VAX for analysis. Thus, the user interface for the RAMS has been tailored for VAX/VMS which ideally takes advantage of the analysis software available (e.g., NCAR Graphics and IMSL).

The RAMS consists of three basic modules: a) a data assimilation package which provides an objective analysis of surface and rawinsonde data which may be used to initialize the model; b) the primary model code; and c) an post processing analysis package which

analyzes and produces graphical displays of model results. It is possible to separate these modules as indicated above such that all assimilation and numerical modeling are conducted on the CRAY, while the analysis is completed on the local VAX. Appendix A describes in more detail some specific aspects of the RAMS system.

Planned RAMS modeling applications include 3-D simulation of individual clouds using a ~30 km horizontal domain, 2-D and 3-D simulations of mesoscale convective systems using horizontally-homogeneous initialization; and 3-D simulations of MCS's using variable input fields based on objective analysis of NMC data and special COHMEX network data. In addition, Dr. Richard McNider of UAH plans to use RAMS for a number of COHMEX case study days of cumulus cloud development.

3. 13 July 1986 COHMEX Analysis Work

The 13 July MCS will probably receive a great deal of attention by several investigators because of its development scenario and ideal location over the heart of the SPACE/COHMEX network. This MCS formed and reached maturity over the COHMEX network, within range of Doppler radars and the surface mesonet. At maturity, the MCS cloud shield exhibited an east-west major axis of 250 km and a N-S minor axis of 150-200 km (see Fig 1). It was composed of a convective leading edge and an adjacent region of stratiform precipitation extending up to 100 km to the rear of the convective leading edge. Interestingly, the orientation of the system was parallel to the environmental shear vector, in contrast to the more typical arrangement perpendicular to the shear vector. Rainfall amounts were widespread, but variable, averaging about 15-20 mm over an area of ~50000 km^2. Lightning was prevalent within this system, and positive discharges were common during the mature stage within the trailing stratiform precipitation.

The MCS of interest formed within a relatively unstable and moist (~50 mm precipitable water) environment having a simple wind shear profile as shown in Fig. 2. The environmental wind shear vector, as mentioned previously, is generally oriented along the E-W direction. The fact that strongest winds are located at low levels in the form of a weak

low-level jet profile gives rise to negative vertical shear from about 65 kPa to the tropopause. The bulk convective Richardson number (Ri_c, defined following Weisman and Klemp, 1982) is relatively high at 176 due to the largeness of the convective available potential energy and the smallness of the wind shear magnitude. Based on this high value of Ri_c, one would expect a relatively transient multicellular storm structure, which indeed was the case.

An evolutionary overview of this system is shown in Fig. 3, a time series of some radar quantities derived from the Nashville RADAP data. A series of 4 complementary RADAP PPI scans is included in Fig. 4 to document the spatial patterns of precipitation distribution within this MCS. The first echo (18 dBZ threshold) within the MCS was recorded near 1630 UTC over the west-central SPACE/COHMEX network. A nearly monotonic areal growth of convective cores (as indicated by the area of 35 dBZ echo in Fig. 3) is analyzed through 2100 UTC, at which time maximum convective activity was attained. It is interesting to note that the *number* of major convective cores (Fig. 3, bottom panel), determined subjectively from the 10 min PPI plots at 0.5 deg elevation, precedes the maximum in convective mass flux. The implication here is that semi-independent cores merged while undergoing intensification. The importance of cloud-scale merger in growth of convective systems over Florida was previously considered by Simpson (1980). Low-level outflow was particularly vigorous on this day, as indicated by surface mesonet which recorded low-level wind speeds in excess of 15 m s^{-1}. Observations by scientists on board the UND Citation aircraft also indicated near damaging winds in the vicinity of intense convection during the developing stages of this MCS.

The series of PPI's in Fig. 4 show in more detail the nature of the MCS development from a cluster of individual echoes at 2000 UTC and before, to a convective line with a region of trailing stratiform precipitation by 2200 UTC. A particularly interesting feature is the areal growth of the anvil at middle to upper levels. This growth is shown by the vertical hatching in Fig. 4, which is derived from the 2.0 deg RADAP scan. At the ranges involved, the received echo represents precipitation within the 5-11 km AGL level. Note that the

development of precipitation within the anvil precedes the appearance of precipitation at the surface, which is seen in the 0.5 deg PPI scan at 2300 UTC (Fig. 4d). By this time the stratiform region was nearly fully developed. A relative minimum in reflectivity separates the relative maximum within the stratiform region and the convective line, which is beyond maximum range at this time. This relative minimum has been termed the reflectivity trough by Smull and Houze (1985).

The growth of the stratiform precipitation region is also portrayed in the time series of the 2.0 deg 18 dBZ echo in Fig. 3 (dashed line) An inflection point the areal rate of growth is seen just before 2100 UTC, after which the growth rate changes to a much greater constant value. This point of inflection nearly coincides with the maximum in convective activity (the 0.5 deg 35 dBZ curve), suggesting a possible cause and effect relationship. As will be discussed in the following, this point of inflection also coincides with the emergence of pronounced mesoscale flows within the stratiform region. This possible relationship will be examined in further detail using the RAMS model during the second year.

As mentioned earlier, total precipitation amounts at the surface averaged around 15-20 mm. Time series characteristics of the rainfall are displayed in Fig. 5. Convective cores appeared to have produced most of the rainfall over the SPACE mesonet; stratiform precipitation was relatively minor. The plots in Fig. 5 represent those stations in which the stratiform precipitation was most substantial. Over this region, about 3-5 mm was delivered from the stratiform precipitation, which represents about 10-20% the total average rainfall. This value is significantly below typical values of 30-50% reported in the literature for tropical squall lines and for midlatitude squall lines (e.g., Johnson and Hamilton, 1988). It is possible that a greater fraction of stratiform rain was generated south of the SPACE mesonet, where raingages are absent. Analysis of radar data should provide a clearer picture of the precipitation distribution between the convective and stratiform

regions. Convective cores produce isolated rainfall totals of near 50 mm, most of which fell over periods less than 30 mm. Thus, rainfall rates exceeding 100 mm h^{-1} were not uncommon.

The three-dimensional precipitation distribution within this MCS has been analyzed using reflectivity from the C-band CP-4 radar. This radar was used, when available to SPACE researchers, to conduct full-volume scans of the MCS. These typically consisted of 360 deg scans ranging from 0.5 to 18.5 deg. Fig. 6a illustrates the distribution of reflectivity within the western segment of the MCS at the 8 km level at 2156 UTC, about one hour after the expansion of precipitation within the anvil was observed. By this time convective cells located along the southern extremity had weakened, and a relatively uniform precipitation field of ~15-20 dBZ exists 70 km to the north. A north-south vertical cross section in Fig. 6b shows that a considerable portion of this anvil precipitation does not extend to the surface at this time.

The expansion of precipitation within the western portion of the MCS (that region shown in Fig. 6a) can be illustrated by a series of vertical cross sections (as in Fig. 6b) in which reflectivity has been averaged over a 70 km east-west segment. Four composite pictures covering the time period 2049-2349 UTC are shown in Fig. 7. The expansion of precipitation within the MCS was accomplished by both discrete propagation and advection produced by mesoscale flows within the anvil. (Recall that the environmental winds of the undisturbed environment were mostly parallel to the major axis of the system.) At 2049 the system was composed primarily of convective cells with little intervening stratiform precipitation. Reflectivity factor within individual convective cells was near a maximum of ~60-65 dBZ. However, the average values in Fig. 7 do not reveal this because of the absence of significant reflectivity between convective cells. There is evidence of discrete propagation at 2049, as shown by the dual maximum in average reflectivity. The overall system movement perpendicular to the environmental winds was accomplished almost entirely by discrete propagation as depicted in Fig. 7. (This propagation was apparently produced by convergence along the relatively vigorous outflow referred to earlier.)

The subsequent cross sections in Fig. 7 reveal the anvil and associated stratiform precipitation expansion seen above in Figs. 4 and 6. By 2157 UTC the convective line of the MCS continued to propagate to the south (towards the left in Fig. 7), while the anvil region simultaneously expanded towards the north, apparently by advection and growth of precipitation at middle to upper levels within the anvil. This pattern continued through 2349 UTC as shown in Fig. 7. By 2258, the stratiform precipitation region had become well-established at low levels, as evidenced by the presence of the radar bright band located near y=-20 and z=4. Expansion of the stratiform area continued until well past 2349 UTC. It is interesting to note that a general decrease in echo top was analyzed in Fig. 7 while the expansion and growth of the stratiform precipitation region occurred. For example, the 0 dBZ contour descends on the average about 2 km from 2157 to 2349. A similar trend is visible in the cloud top IR temperature patterns (Fig. 1), which show a uniform temperature increase from 2200 to 2300 UTC in both the convective and stratiform regions. The relationship and physical connection between cloud and echo tope will be examined in the future with additional analysis and numerical modeling efforts.

The early growth and expansion of precipitation within the MCS anvil was examined in more detail by calculating the rate of growth of echo between 2122 and 2156 UTC. Fig. 8 shows two vertical sections of average reflectivity, calculated as in Fig. 7, except the vertical stretching factor has been reduced from 3 to 2. The bottom panel of Fig. 8 is the difference in reflectivity from the two periods, i.e, dBZ(2156) - dBZ(2122). The overall maximum of 33.7 dBZ near y=-35 and z=2 is simply from propagation effects within the convective region. A secondary maximum near y=50, z=10 is due primarily to advection of anvil precipitation by an induced mesoscale outflow jet, which was directed from south to north. This jet is described in further detail below. Of greater interest is the band of reflectivity increase between y=-5 and y=40 at heights of 5-10 km. It is within this region where in situ growth of precipitation appears to be occurring at a rate of ~10-15 dBZ h^{-1}. This warrants further study and analysis because this result differs in principle from previous studies, in which direct particle transfer from the convective region to the stratiform

region has been inferred (e.g., Rutledge and Houze, 1987). In the present case, much of the increase in reflectivity (precipitation growth) occurs within a temperature range of -10 to -30 ^{o}C.

As mentioned above, the expansion of anvil/stratiform precipitation within this MCS was associated with induced mesoscale flows, particularly in the direction normal to the major axis of the system. Fig. 9 shows the flow patterns derived from the 2156 analysis time considered above. The v wind profile shown in the lower right panel of Fig. 9 reveals an inflow jet of -9 m s^{-1} magnitude within the rear portion of the system (the averages were taken from y = 10 to y = 40 as shown) below 8 km. Above this is an outflow jet of +6 m s^{-1} magnitude. This wind profile represents a mesoscale response, since such winds are not visible in the pre-storm sounding of Fig. 2. Such winds were important in the growth and distribution of stratiform precipitation in this case, as demonstrated above. At later times, the v profile appeared to change even further. The lower left panel in Fig. 9 represents an approximate distribution of the u velocity component, averaged over the x interval -100 to -40. This distribution exhibits much structure, particularly in the vicinity of the convective line, which is typically the case. Maximum values of > 10 m s^{-1} (flow from the west or into Fig. 9) are found near y = -30, z = 8. A flow reversal is located above z = 12 and is particularly prominent at high levels in advance of the line (near y = -40, z = 13). Thus, the wind component along the major axis of the system is appreciable and exhibits considerable structural variability. Such structural variability in winds needs to be closely considered in calculation of precipitation trajectories.

Future work on this case will expand on the precipitation and kinematic analyses presented above. In particular, the following tasks are planned for the second year:

- o complete interpolation of all reflectivity data to a Cartesian grid;
- o conduct a VAD analysis of all 360 deg scans to derive mesoscale flow fields, including vertical motion;
- o analyze the wind profiler data to get vertical air motion in addition to estimates of precipitation terminal fall speeds;

- o conduct some analyses of CP-2 multiparameter data to make inferences on the characteristics of precipitation with the MCS;
- o conduct some multiple Doppler analyses to characterize the structure of the convective components within this MCS;
- o begin work on numerical modeling of individual convective clouds comprising the MCS, and on simulation of the MCS itself, in both 2-D and 3-D;
- o extend the satellite analyses to (i) examine the merging process seen in the GOES data, (ii) examine the behavior of cloud top and (iii) merge the results of of (i) and (ii) with analyses of other data sets.

Completion of these tasks will be done in close collaboration with Steve Goodman, Patrick Wright and Dennis Beuchler of USRA, who will be investigating the relationship between electrical activity and the kinematic and precipitation structure of this MCS.

4. Preliminary survey of the 15 July MCS

A small MCS formed during the early morning hours (~0900 UTC) over the SPACE network and moved just beyond the southern extremity of the network where it dissipated near 2000 UTC. At maturity, this circular system was about 100 in diameter and was striking in its stratiform nature. Although convective cores were present, stratiform precipitation appeared to contribute a major fraction of the precipitation from this long-lived and relatively small system. As in the previous case, the system moved over the heart of the COHMEX mesonet, so abundant radar data are available for analysis. Analyses of this system to be conducted during the second year will provide significant contrast to the 13 July case described above.

References

Johnson, R.H., and P.J. Hamilton, 1988: The relationship of surface pressure features to the precipitation air flow structure of an intense midlatitude squall line. *Mon. Wea. Rev.*, **116**, 1444-1472.

Rutledge, S.A., and R.A. Houze, 1987: A diagnostic modeling study of the trailing stratiform region of a midlatitude squall line. *J. Atmos. Sci.*, **44**, 2640-2656.

Simpson, J., 1980: Downdrafts as linkages in dynamic cumulus seeding effects. *J. Appl. Meteor.*, **19**, 477-487.

Smull, B.F., and R.A. Houze, 1985: A midlatitude squall line with a trailing region of stratiform precipitation: Radar and satellite observations. *Mon. Wea. Rev.*, **113**, 117-133.

Weisman, M.L., and J.B. Klemp, 1984: The structure and classification of numerically simulated convective storms in directionally varying wind shears. *Mon. Wea. Rev.*, **112**, 2479-2498.

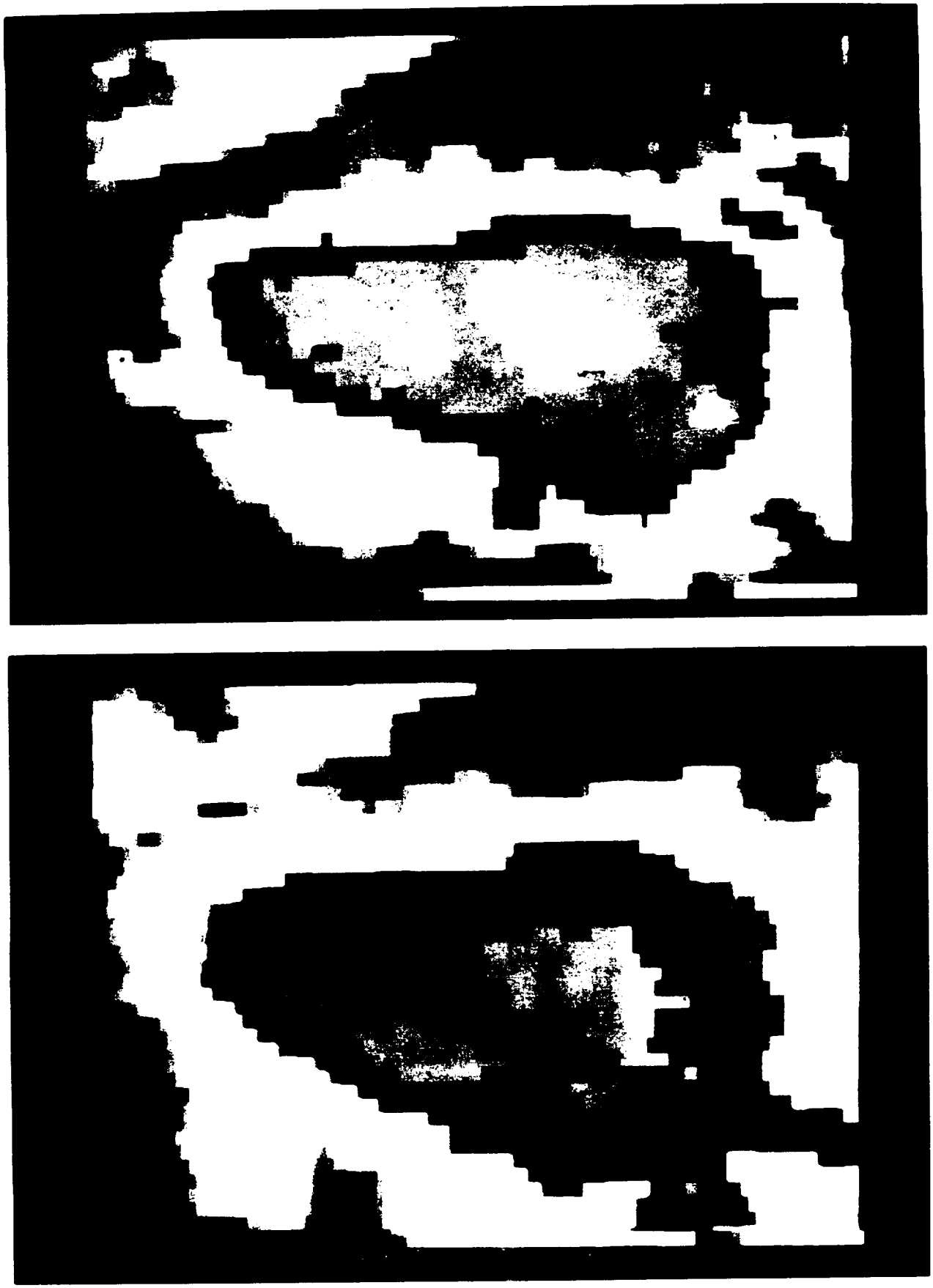

Figure 1. GOES IR images for 2200 and 2300 UTC, 13 July 1986. An MB enhancement has been applied.

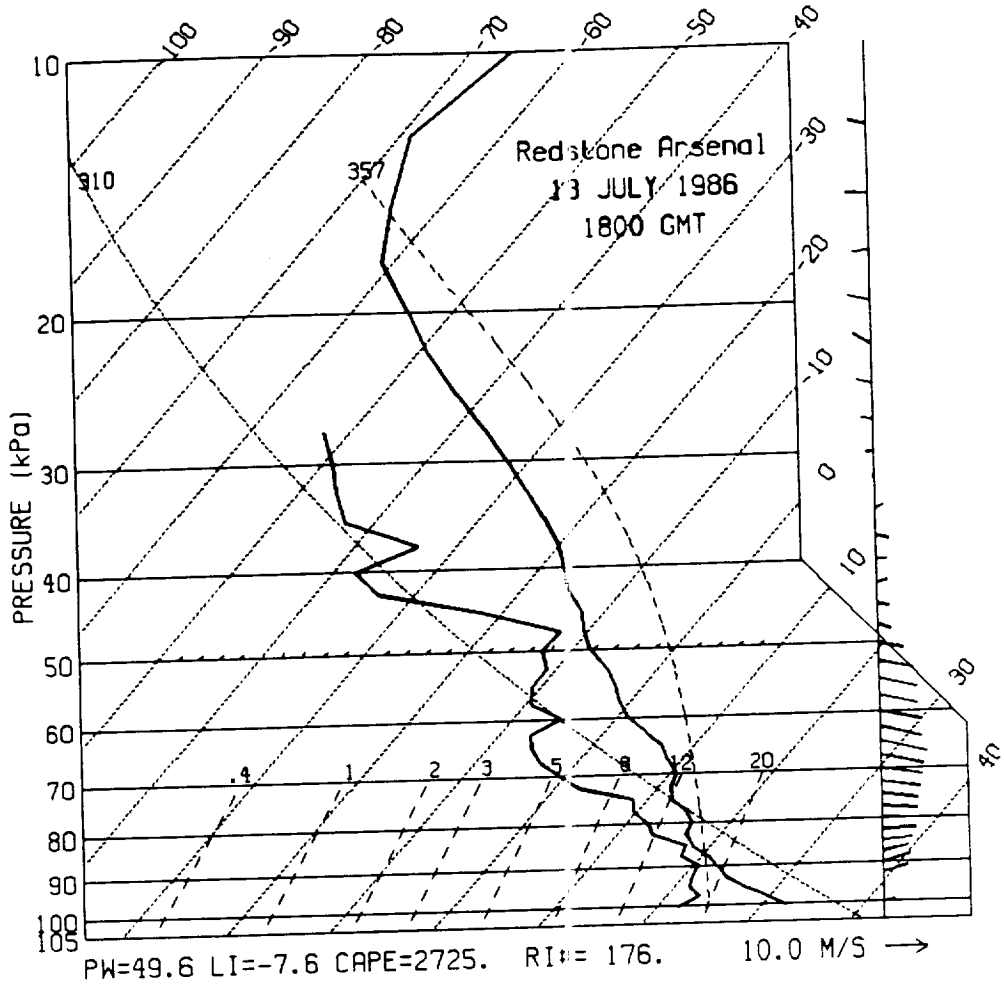

Figure 2. Rawinsonde sounding taken from Redstone arsenal at 1800 UTC 13 July 1986. The actual sounding release time was 1730 UTC, about one hour after first echos were observed in the developing MCS located about 80 km NW of the sounding site at this time.

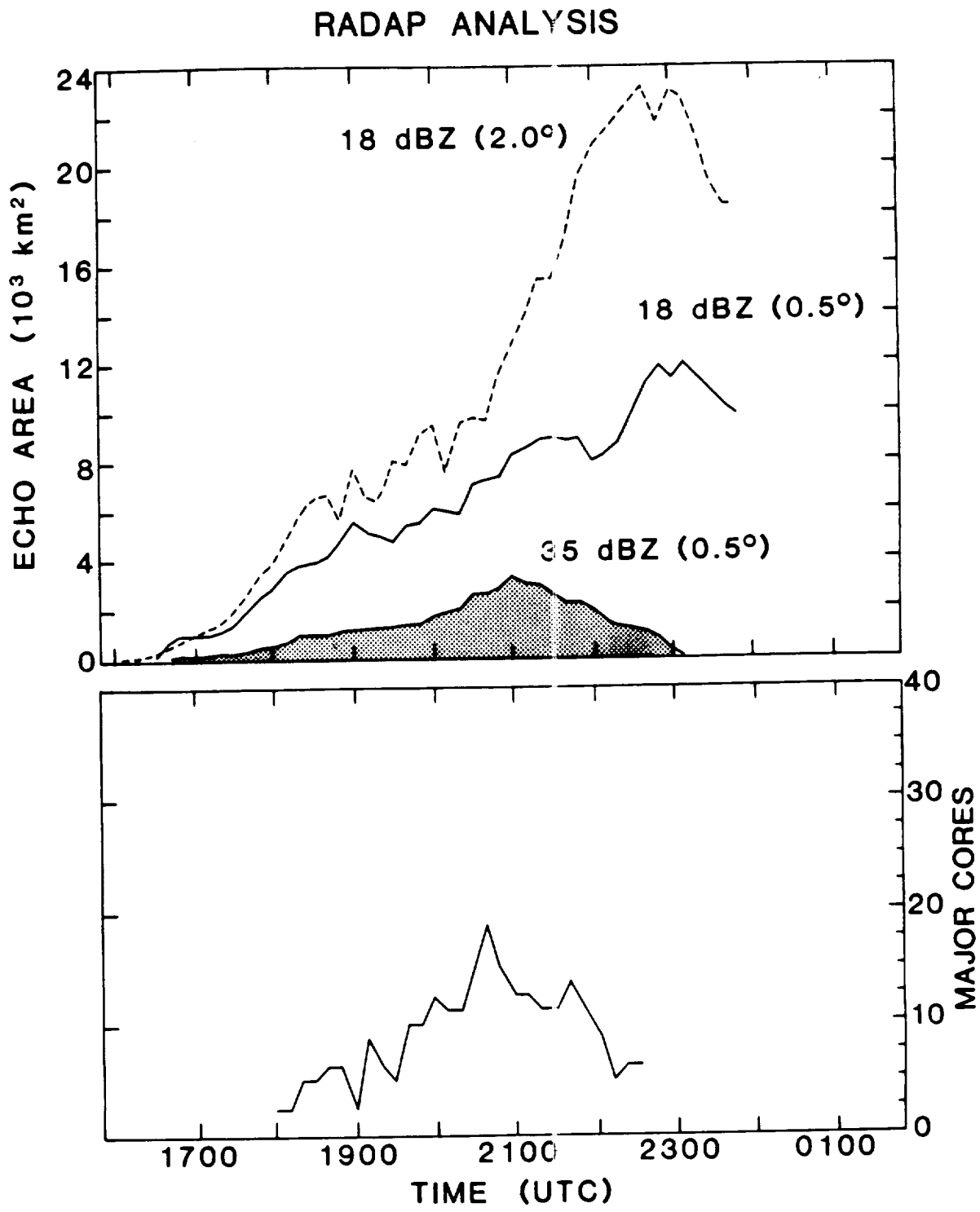

Figure 3. Time series of echo quantities derived from the RADAP data, which are acquired at 10 min time intervals. The top panel gives areas within given echo contours at given elevations,while the bottom panel is a subjective determination of the number of major convective cores.

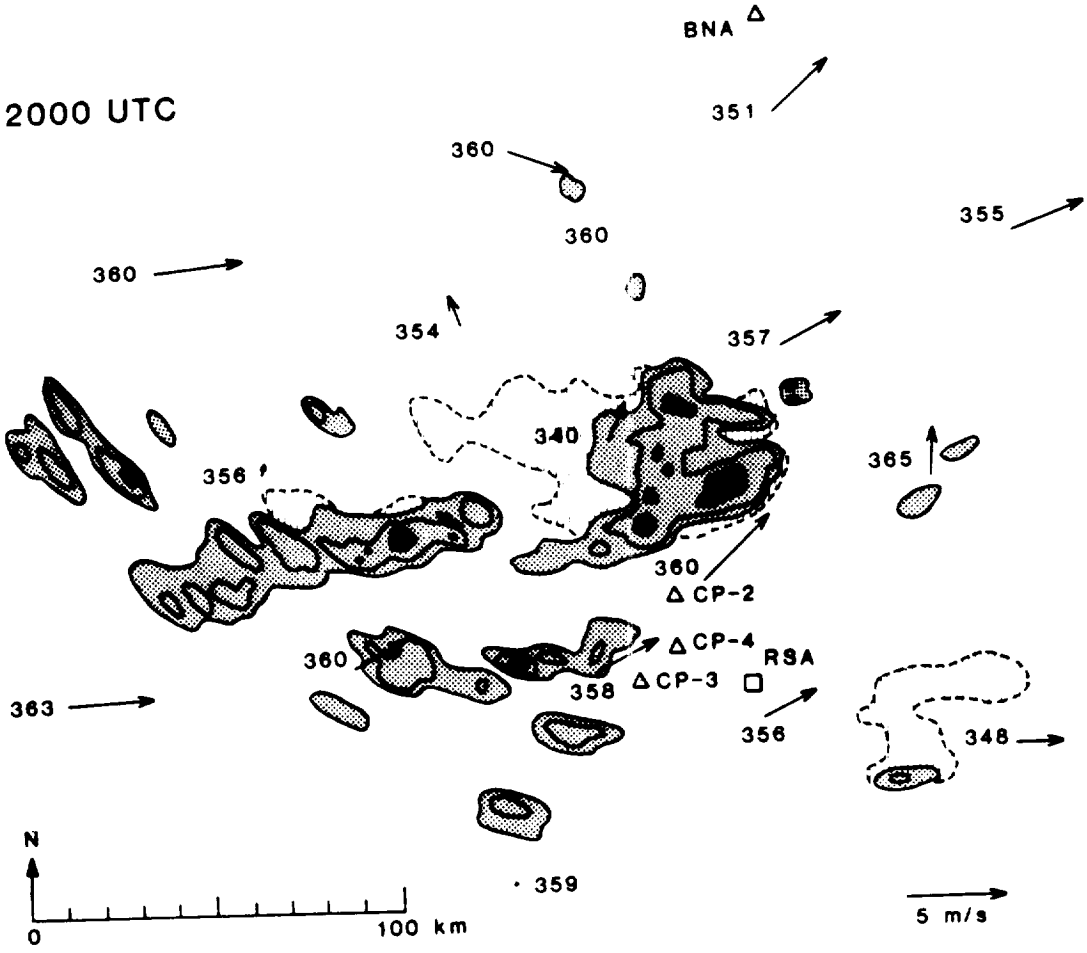

Figure 4a. PPI analysis of RADAP data for 2000 UTC, 13 July 1986. Echo contours are drawn at 18, 30 and 43 dBZ. Echo intensities greater than 43 dBZ are black. Vertical hatching depicts reflectivity factor > 18 dBZ on the 2.0 deg PPI scan, which intersects the MCS at the middle to upper levels (5-11 km), and shows the development of precipitation within the anvil region of the MCS. Surface data consisting of winds and equivalent potential temperature are plotted.

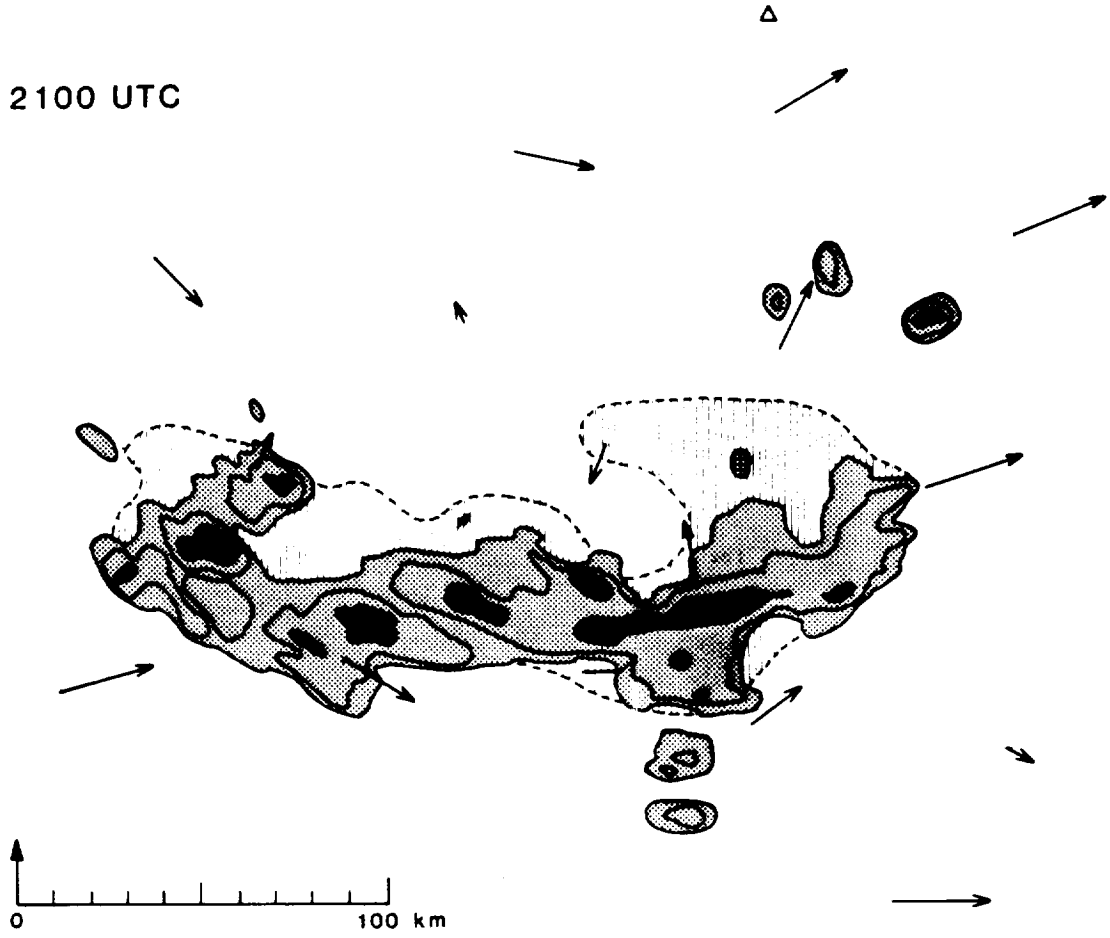

Figure 4b. Same as Fig. 4a, except for 2100 UTC.

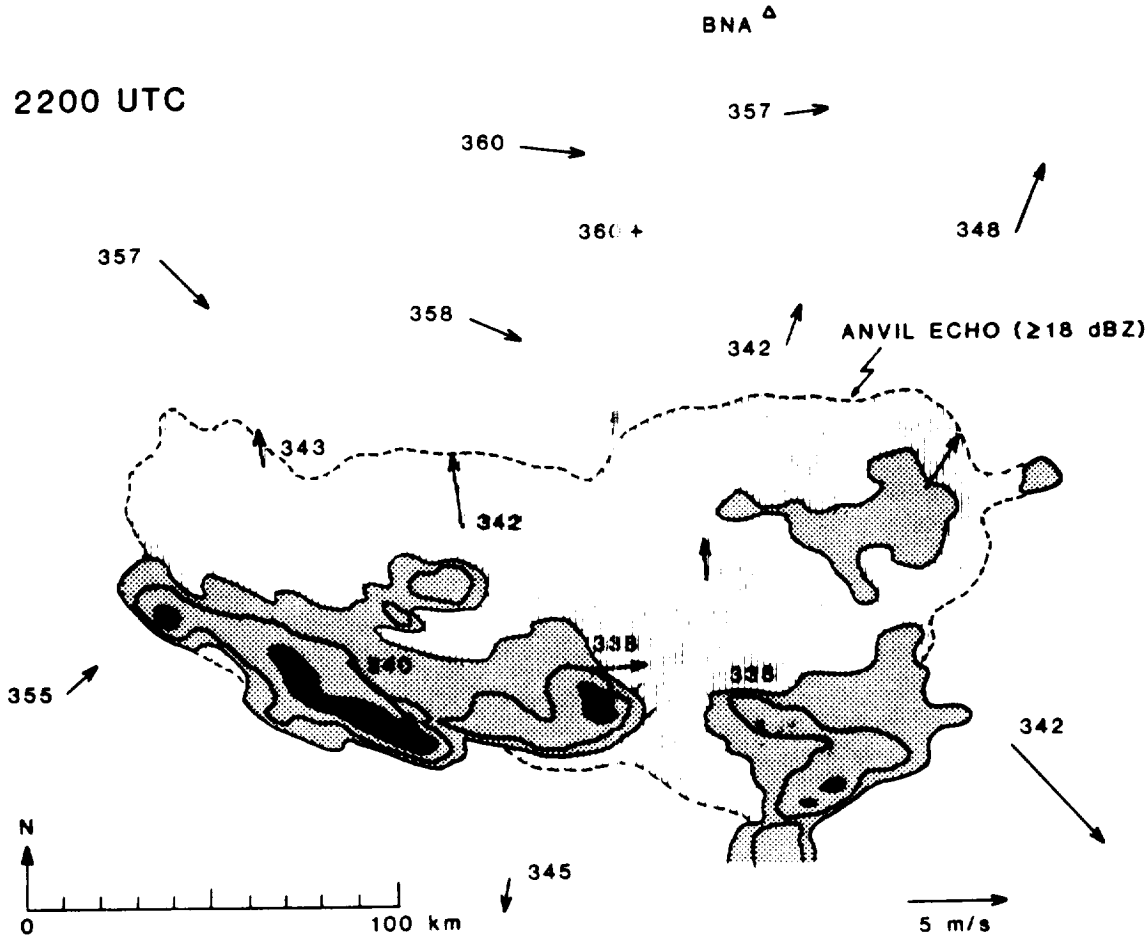

Figure 4c. Same as Fig. 4a, except for 2200 UTC.

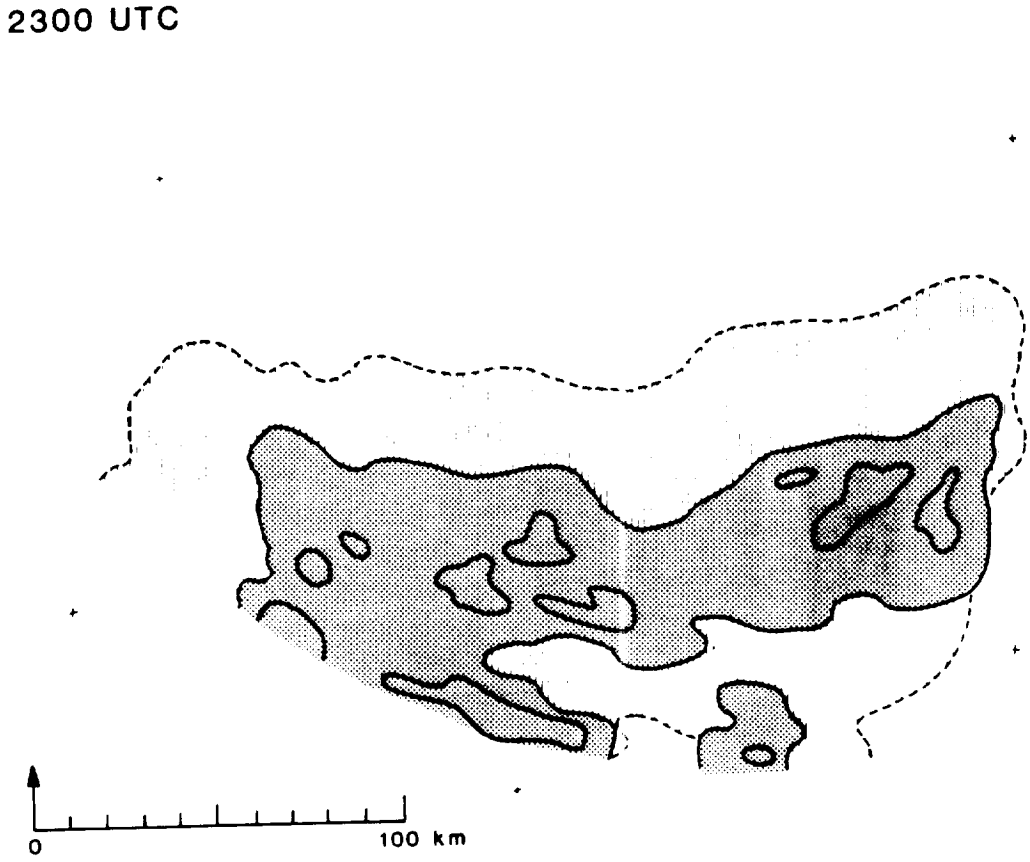

Figure 4d. Same as Fig. 4a, except for 2300 UTC.

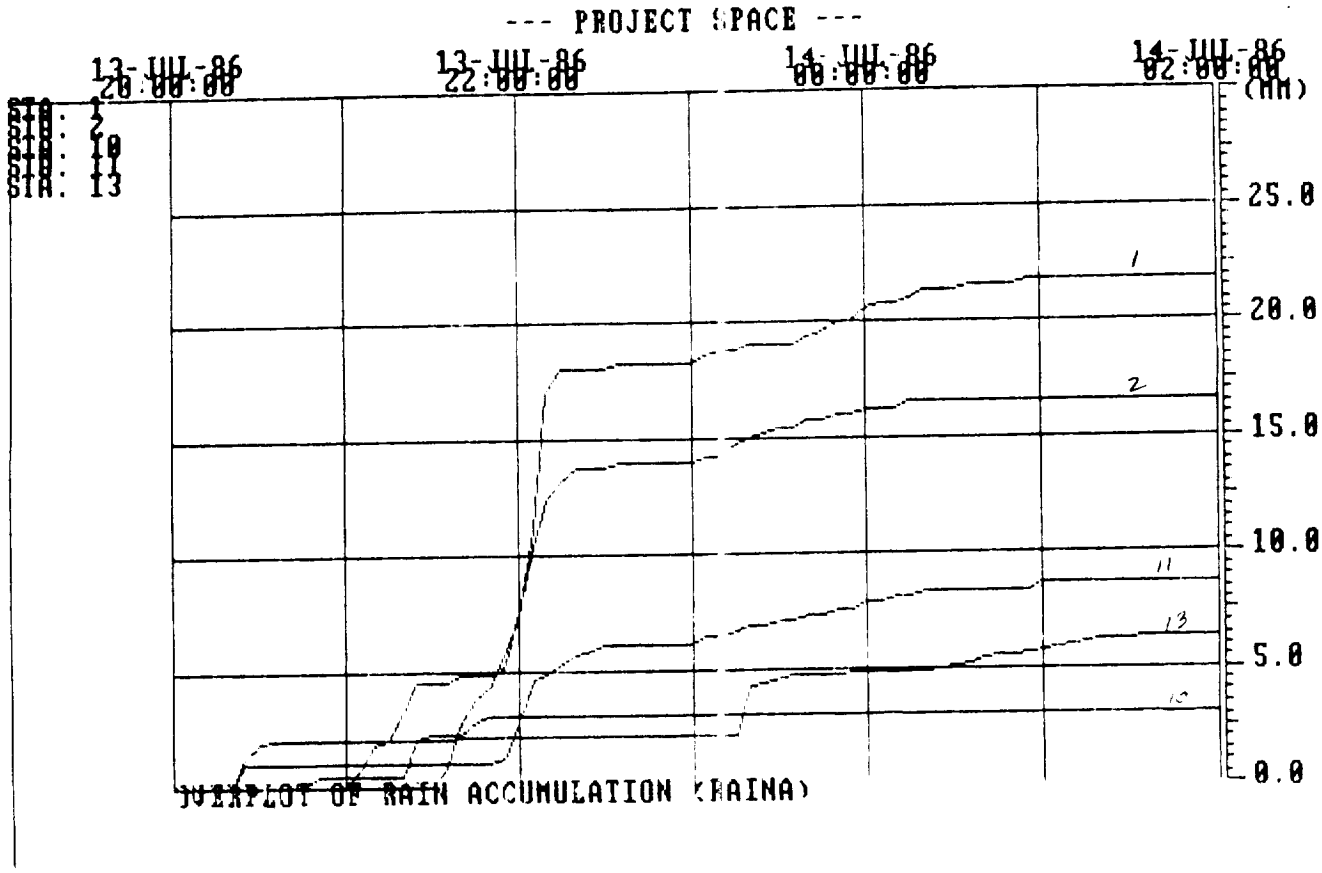

Figure 5. Time series of accumulated precipitation (mm) from mesonet stations 1, 2, 10, 11, and 13, all located over the southern to south central portion of the SPACE mesonet.

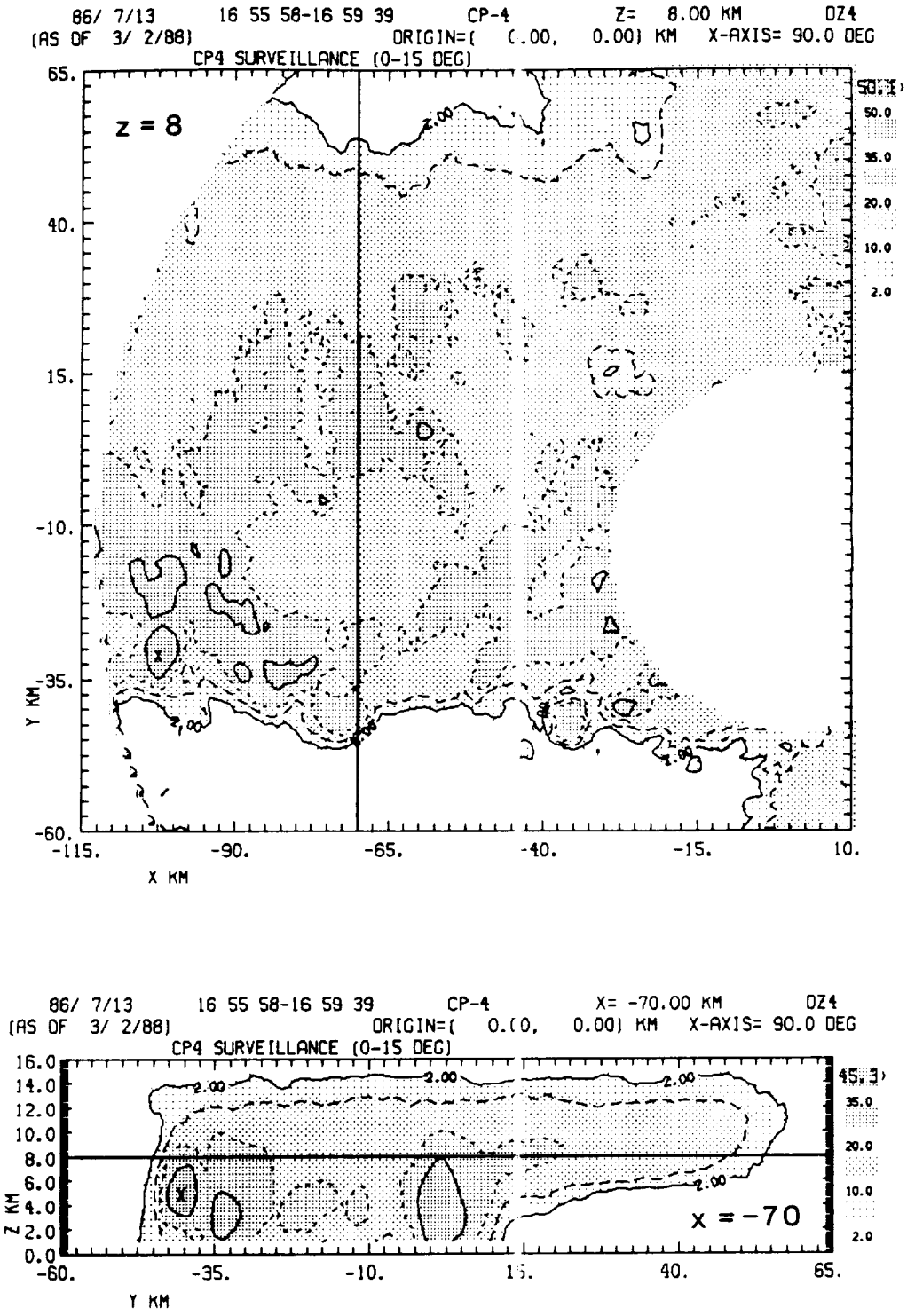

Figure 6. Analysis of CP-4 reflectivity data on (a) the z=8 km plane, and (b) the y=-70 km plane for 2156 UTC. Contours are drawn at 2, 10, 20, 35 and 50 dBZ.

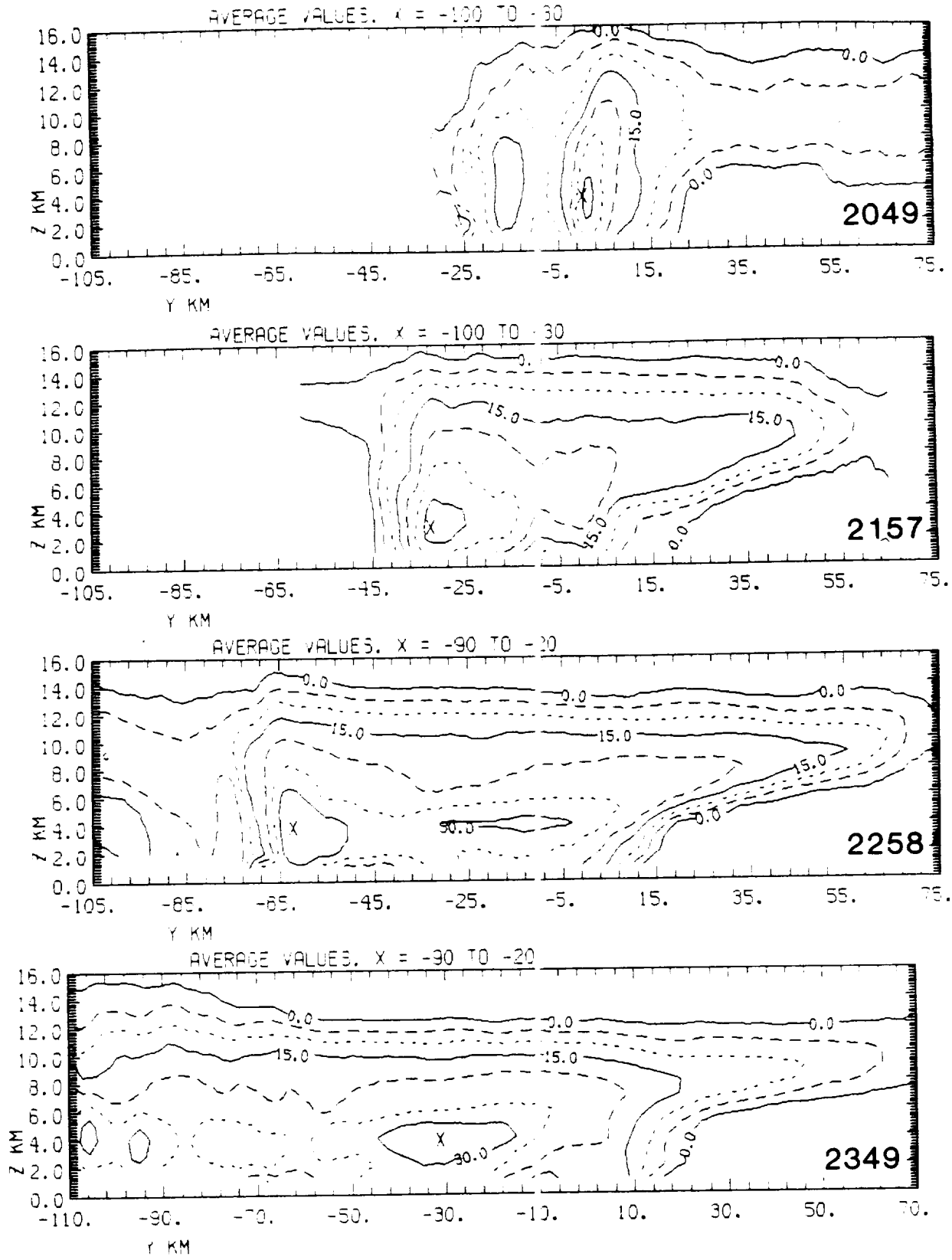

Figure 7. East-west averages of CP-4 reflectivity fa(tor at 2049, 2157, 2258 and 2349 UTC. The x interval of the averages is indicated at the top of each panel. See Fig. 6 for relative location of the averages with respect to the MCS.

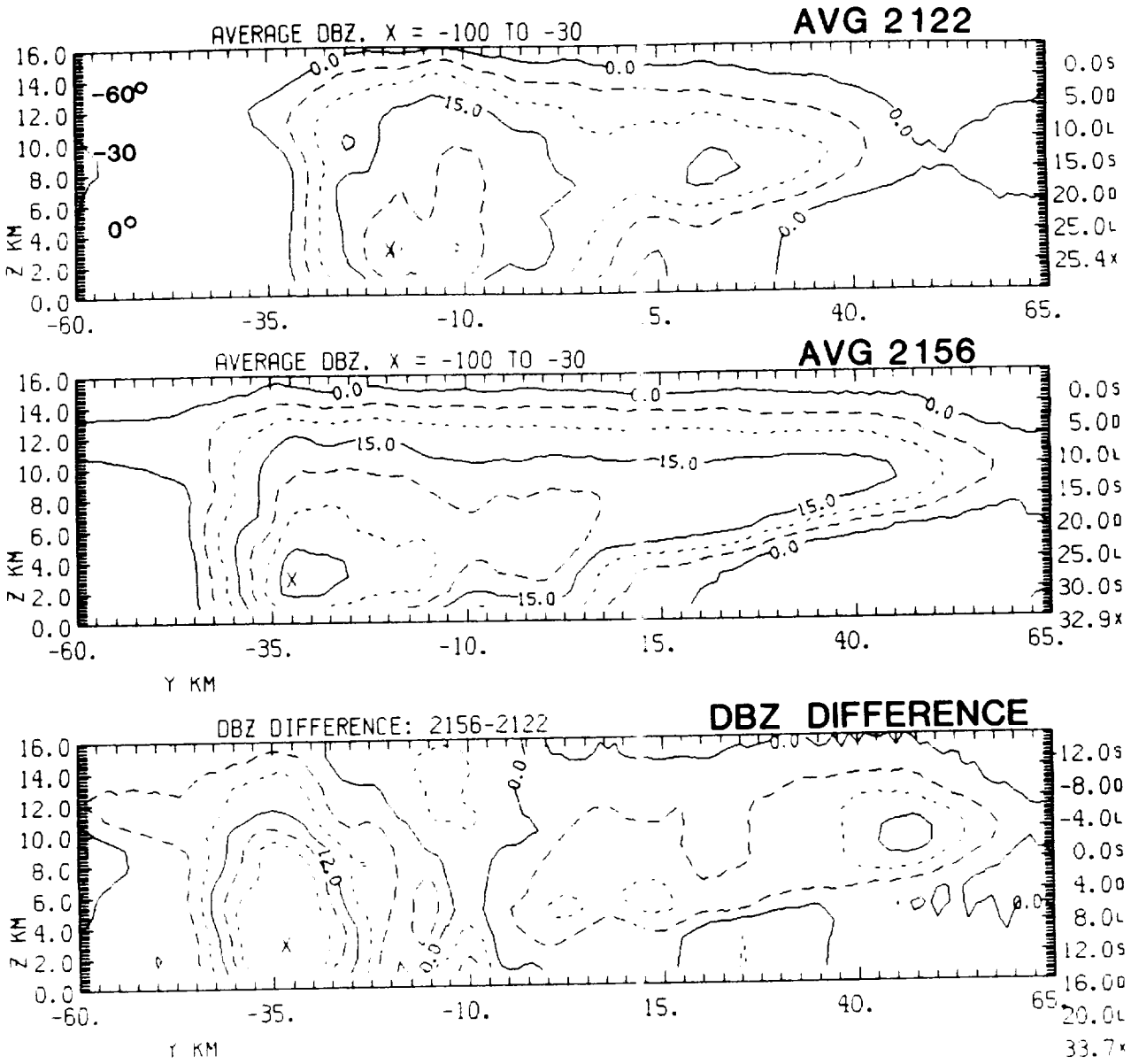

Figure 8. The top two panels are averages of CP-4 reflectivity as in Fig. 7. The bottom panel represents the difference in dBZ between the top two panels.

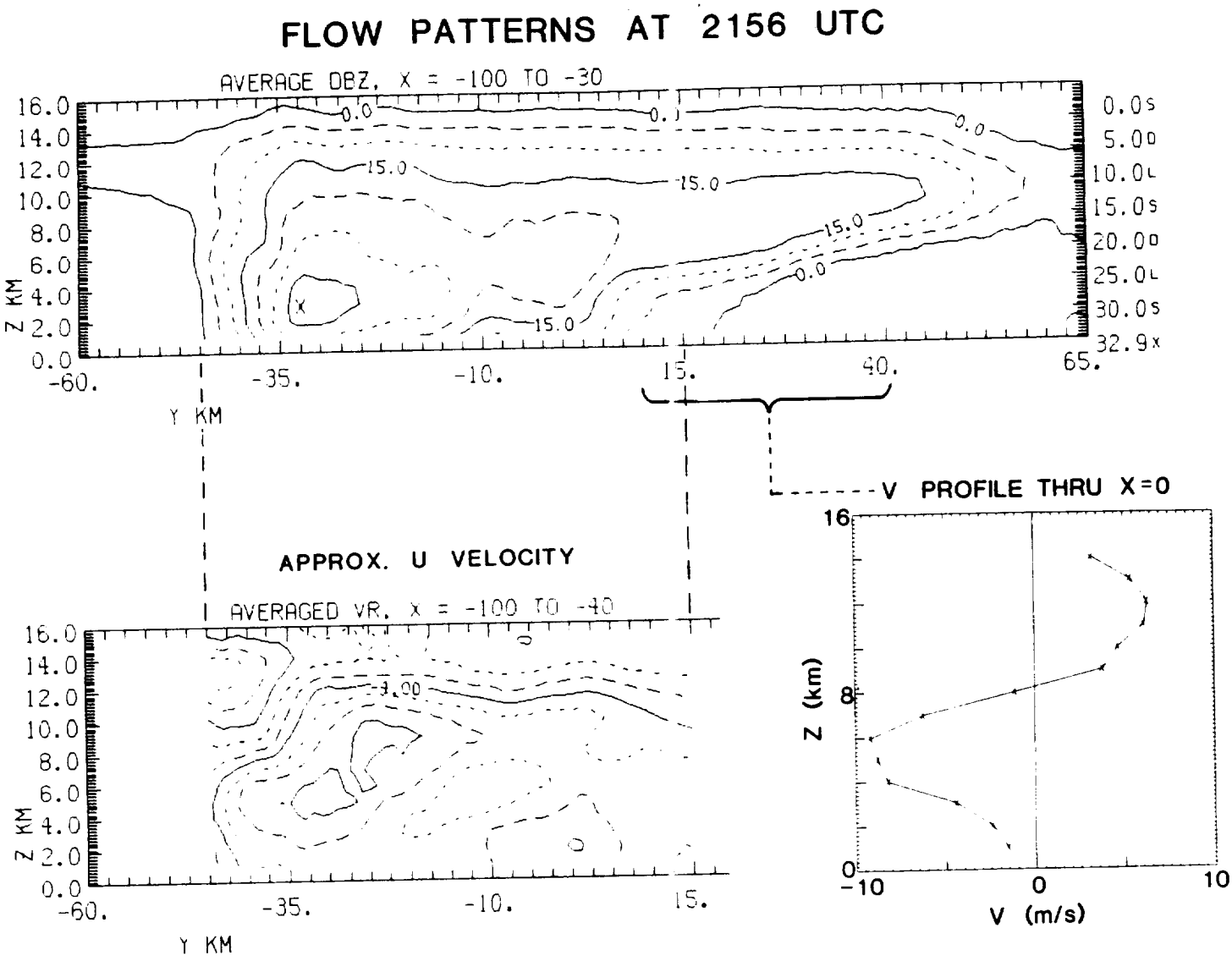

Figure 9. Analysis of kinematic quantities at 2156 UTC. The top panel is averaged reflectivity as in Figs 7 and 8. The bottom right panel is the v wind component acquired from CP-4 radial velocity data along the N-S line passing through CP-4, averaged over the y = 10 to y = 40 interval. The bottom left panel is the approximate u velocity, derived from an average of radial velocity over the x = -100 to x = -40 interval.

Appendix A. Description the the Regional Atmospheric Modeling System (RAMS)

THE CSU RAMS

INTRODUCTION

The numerical atmospheric models developed independently under the direction of William R. Cotton and Roger A. Pielke have recently been combined into the CSU Regional Atmospheric Modelling System (RAMS). Development of many of the physical modules has been accomplished over the past 15 years and has involved over 50 man years of effort. RAMS is a general and flexible modelling system rather than a single purpose model. For example, current research using RAMS includes atmospheric scales ranging from large eddy simulations ($\Delta \approx 100\ m$) to mesoscale simulations of convective systems ($\Delta x \approx 100 km$). This paper will discuss the options available in RAMS, the engineering aspects of the system and how the flexibility is attained.

RAMS OPTIONS

RAMS is a merging of basically three models that were designed to simulate different atmospheric circulations. These were a non-hydrostatic cloud model (Tripoli and Cotton, 1982) and two hydrostatic mesoscale models (Tremback *et al.*, 1985 and Mahrer and Pielke, 1977). The capability of RAMS was recently augmented with the implementation of 2-way interactive grid nesting. Because of this, the modelling system contains many options for various physical and numerical processes. These options are listed below.

The following options are currently available in configuring a model:

1. Basic equations:

   Option 1 Non-hydrostatic time-split compressible (Tripoli and Cotton, 1980)

   Option 2 Hydrostatic incompressible or compressible (Tremback *et al.*, 1985)

2. Dimensionality: 1, 2, or 3 spatial dimensions

3. Vertical coordinate:

   Option 1 Standard cartesian

   Option 2 Sigma-z

4. Horizontal coordinate:

   Option 1 Standard cartesian

   Option 2 Latitude/longitude

5. Grid Structure:

   - Arakawa-C grid stagger
   - Unlimited number of nested grids
   - Unlimited number of levels of nesting

6. Finite differencing:

Option 1 leapfrog on long timestep, forward-backward on small timestep, 2nd or 4th order flux conservative advection.

Option 2 forward-backward time split, 6th order flux conservative (Tremback *et al.*, 1987)

7. Turbulence closure:

Option 1 Smagorinsky-type eddy viscosity with R_i dependence

Option 2 Level 2.5 type closure using eddy viscosity as a function of a prognostic turbulent kinetic energy

Option 3 O'Brien profile function in a convective boundary layer (Mahrer and Pielke, 1977); local exchange coefficient in a stable boundary layer (McNider, 1981).

8. Condensation

Option 1 Grid points fully saturated or unsaturated

Option 2 No condensation

9. Cloud microphysics

Option 1 Warm rain conversion and accretion of cloud water (r_c) to raindrops (r_r), evaporation and sedimentation (Tripoli and Cotton, 1980)

Option 2 Option 1 plus specified nucleation of ice crystals (r_i), conversion nucleation and accretion of graupel (r_g), growth of ice crystals (r_i), evaporation, melting and sedimentation (see Cotton *et al.*, 1982)

Option 3 Option 1 plus option 2 plus predicted nucleation and sink of crystal concentration (N_i), conversion and growth of aggregates (r_a), melting, evaporation and sedimenation (see accompanying flow diagram, Figure 1). The nucleation model includes: sorption/deposition, contact nucleation by Brownian collision plus thermophoresis plus diffusiophoresis, secondary ice crystal production by rime-splinter mechanism.

Option 4 No precipitation processes

10. Radiation:

Option 1 Shortwave radiation model including molecular scattering, absorption of clear air (Yamamoto, 1962), ozone absorption (Lacis and Hansen, 1974) and reflectance, transmittance and absorptance of a cloud layer (Stephens, 1978), clear-cloudy mixed layer approach (Stephens, 1977)

Option 2 Shortwave radiation model described by Mahrer and Pielke (1977) which includes the effects of forward Rayleigh scattering (Atwater and Brown, 1974), absorption by water vapor (McDonald, 1960), and terrain slope (Kondrat'yev, 1969).

Option 3 Longwave radiation model including emissivity of a clear atmosphere (Rodgers, 1967), emissivity of cloud layer (Stephens, 1978), and emissivity of "clear and cloudy" mixed layer (Herman and Goody, 1976)

Option 4 Longwave radiation model described by Mahrer and Pielke (1977) including emissivities of water vapor (Jacobs *et al.*, 1974) and carbon dioxide (Kondrat'yev, 1969) and the computationally efficient technique of Sasamori (1972).

Option 5 No radiation

11. Transport and diffusion modules:

Option 1 Advection-diffusion model (Segal *et al.*, 1980) (To be implemented.)

Option 2 Semi-stochastic particle model for point and line sources of pollution (McNider, 1981) (To be implemented.)

12. Lower boundary:

Option 1 Specified surface temperature and moisture function or specified surface fluxes coupled with constant flux layer condition based on similarity theory (Manton and Cotton, 1977)

Option 2 Surface layer temperature and moisture fluxes are diagnosed as a function of the ground surface temperature derived from a surface energy balance (Mahrer and Pielke, 1977). The energy balance includes longwave and shortwave radiative fluxes, latent and sensible heat fluxes, and conduction from below the surface. To include the latter effect, a multi-level prognostic soil temperature model is computed.

Option 3 Modified form of Option 2 with prognostic surface equations (Tremback and Kessler, 1985)

Option 4 Same as Option 2, except vegetation parameterizations are included (McCumber and Pielke, 1981; 1984; McCumber, 1980) (To be implemented)

13. Upper boundary conditions:

Option 1 Rigid lid

Option 2 Rayleigh Friction layer plus Option 1-4

Option 3 Prognostic surface pressure (hydrostatic only)

Option 4 Material surface top. (hydrostatic only) (Mahrer and Pielke, 1977)

Option 5 Gravity wave radiation condition (Klemp and Durran, 1983)

14. Lateral boundary conditions:

Option 1 Klemp and Wilhelmson (1978) radiative boundary conditions

Option 2 Orlanski (1976) radiative boundary conditions

Option 3 Klemp and Lilly (1978) radiative boundary condition

Option 4 Option 1, 2 or 3 coupled with Mesoscale Compensation Region (MCR) described by Tripoli and Cotton (1982) with fixed conditions at MCR boundary (see Figure 2)

Option 5 The sponge boundary condition of Perkey and Kreitzberg (1976) when large scale data is available from objectively analyzed data fields or a larger scale model run. This condition includes a viscous region and the introduction of the large scale fields into the model computations near the lateral boundaries.

15. Initialization

Option 1 Horizontally homogeneous.

Option 2 Option 1 plus variations to force cloud initiation.

Option 3 NMC data and/or soundings objectively analyzed on isentropic surface and interpolated to the model grid.

Option 4 NMC data interpolated to the model grid.

As one can see, RAMS is quite a versatile modelling system. RAMS has been applied to the simulation of the following weather phenomena.

1. Towering cumuli and their modification
2. Mature tropical and mid-latitude cumulonimbi
3. Dry mountain slope and valley circulations
4. Orographic cloud formation
5. Marine stratocumulus clouds
6. Sea breeze circulations
7. Mountain wave flow
8. Large eddy simulation of power plant plume dispersal
9. Urban circulations
10. Lake effect storms
11. Tropical and mid-latitude convective systems

ENGINEERING ASPECTS

Because of the large number of options in RAMS, the structuring of the code needs to be carefully considered. This section will discuss various aspects of the code structure of the system.

Pre-processor The code of RAMS is written in as close to the FORTRAN 77 standard as possible. However, with a program as large as this, the FORTRAN standard is lacking in several features such as global PARAMETER and COMMON statements and conditional compilation. To remedy these insufficiencies, the RAMS code takes advantage of a pre-processor written as part of the RAMS package. This pre-processor itself is written in the 77 standard so that the package as a whole is highly portable. It takes full advantage of the character features of FORTRAN and has executed successfully on a number of machines including a VAX, CRAY-1, CRAY-X-MP, and CYBER 205 without modification. Some of the features of the pre-processor are described below:

1) By including a character in the first column of a line of code, that line can be "activated" or "eliminated" from the compile file. This allows for conditional compilation of single lines or entire sections of code.

2) A pre-processor variable can be set to a value. This variable can then be used in other expressions including a pre-processor IF or block IF to conditionally set other pre-processor variables. These variables also can be converted to FORTRAN PARAMETER statements which can be inserted anywhere in the rest of the code.

3) A group of statements can be delineated as a "global" which then can be inserted anywhere in the code. This is very useful for groups of COMMON and PARAMETER statements.

4) DO loops can be constructed in a DO/ENDDO syntax, eliminating the need for statement labels on the DO loops.

Two-way interactive grid nesting The use of grid nesting allows a wider range of motion scales to be modeled simultaneously and interactively. It can greatly ease the limitations of unnested simulations in which a compromise must be reached between covering an adequately large spatial domain and obtaining sufficient resolution of a particular local phenomenon. With nesting, RAMS can now feasibly model mesoscale circulations in a large domain where low resolution is adequate, and at the same time resolve the large eddy structure within a cumulus cloud in a subdomain of the simulation.

Nesting in RAMS is set up such that the same model code for each physical process such as advection is used for each grid. This makes it easy for any desired number of grids to be used without having to duplicate code for each one. Also, it is easy to add or remove a nested grid in time, and to change its size or location. There is still the flexibility of choosing many model options independently for different grids.

RAMS has adopted the two-way interactive nesting procedure described in Clark and Farley (1979). This algorithm is the means by which the different nested grids communicate with each other. The process of advancing coarse grid A and fine nested grid B forward in time one step begins with advancing grid A alone as if it contained no nest within. The computed fields from A are then interpolated tri-quadratically to the boundary points of B. The interior of B is then updated under the influence of its interpolated boundary values. Finally, the field values of A in the region where B exists are replaced by local averages from the fields of B. An increase in efficiency over the Clark and Farley method was implemented by allowing a coarse grid to be run at a longer timestep than a fine grid.

The following options are available with nesting in RAMS:

1) There is no imposed limit (only a practical one) to the number of nested grids which can be used.

2) When two grids B and C are nested within grid A, they may be either independent (occupying different space) or C may be nested within B.

3) The increase in spatial resolution of a nested grid may be any integer multiple of its parent grid resolution. Moreover, this multiple may be specified independently for the three coordinate directions.

4) A nested grid may, but need not, start from the ground and extend to the model domain top.

I/O structure For those machines with limited central memory and a "non-virtual" operating system or for efficiency on virtual systems, RAMS is constructed with a disk I/O scheme. When the scheme is operating, a subset of the model's three-dimensional variables will reside in central memory at any one time. Computations then can be performed with this subset. When these computations are finished, a new subset of three-dimensional variables are requested and computations performed with these. The RAMS structure, thus, is dependent on this I/O scheme and consists of a series of calls to the I/O scheme and to the routines which do the calculations.

Modularity For flexibility, RAMS is written as modular as possible. Each individual physical parameterization or numerical process is put in a separate subroutine so that the routines can easily be replaced for different options or with new developments.

Computational routines The routines that do the actual computations for the model are written so that the implementor of a new or replacement routine does not need to be concerned with most of the details of the rest of the model computations. All three-dimensional variables are "passed" to the subroutines through the call statement with other variables passed through COMMON. The implementor then has the flexibility to structure his routine in whatever manner he wishes to produce the desired result. This concept will also make the implementation of routines from other models and programs easier with less modification required.

Analyais rountines A set of subroutines has been developed for analyzing and plotting a variety of quantities from fields output from RAMS. This greatly facilitiates the interpretation and understanding of modeled atmospheric phenomena. The quantities diagnosed by these routines include vorticity, divergence, streamfunction, energy, momentum flux, most variances and covariances, and layer averaged quantities.

REFERENCES

Atwater, M.A. and P.S. Brown, Jr., 1974: Numerical calculation of the latitudinal variation of solar radiation for an atmosphere of varying opacity. *J. Appl. Meteor.*, **13**, 289-297.

Cotton, W.R., M.A. Stephens, T. Nehrkorn, and G.J. Tripoli, 1982: The Colorado State University three-dimensional cloud/mesoscale model - 1982. Part II: An ice phase parameterization. *J. de Rech. Atmos.*, **16**, 295-320.

Herman, G. and R. Goody, 1976: Formation and persistence of summertime arctic stratus clouds. *J. Atmos. Sci.*, **33**, 1537-1553.

Jacobs,C.A., J.P. Pandolfo and M.A. Atwater, 1974: A description of a general three dimensional numerical simulation model of a coupled air-water and/or air-land boundary layer. IFYGL final report, CEM Report No. 5131-509a.

Klemp, J.B. and D.R. Durran, 1983: An upper boundary condition permitting internal gravity wave radiation in numerical mesoscale models. *Mon. Wea. Rev.*, 111, 430-444.

Klemp, J.B. and R.B. Wilhelmson, 1978a: The simulation of three-dimensional convective storm dynamics. *J. Atmos. Sci.*, 35, 1070-1096.

Klemp, J.B. and R.B. Wilhelmson, 1978b: Simulations of right- and left-moving storms produced through storm splitting. *J. Atmos. Sci.*, 35, 1097-1110.

Klemp, J.B. and D.K. Lilly, 1978: Numerical simulation of hydrostatic mountain waves. *J. Atmos. Sci.*, 35, 78-107.

Kondrat'yev, J., 1969: *Radiation in the Atmosphere.* Academic Press, New York, 912 pp.

Lacis, A.A., and J. Hansen, 1974: A parameterization for the absorption of solar radiation in earth's atmosphere. *J. Atmos. Sci.*, 31, 118-133.

Mahrer, Y. and R.A. Pielke, 1977: A numerical study of the airflow over irregular terrain. *Beitrage zur Physik der Atmosphare*, 50, 98-113.

Manton, M.J., and W.R. Cotton, 1977: Parameterization of the atmospheric surface layer. *J. Atmos. Sci.*, 34, 331-334.

McCumber, M.D., 1980: A numerical simulation of the influence of heat and moisture fluxes upon mesoscale circulation. Ph.D. dissertation, Dept. of Environmental Science, University of Virginia.

McCumber, M.C. and R.A. Pielke, 1981: Simulation of the effects of surface fluxes of heat and moisture in a mesoscale numerical model. Part I: Soil layer. *J. Geophys. Res.*, 86, 9929-9938.

McCumber, M.C. and R.A. Pielke, 1983: Simulation of the Effects of Surface Fluxes of Heat and Moisture in a Mesoscale Numerical Model. Part 2: Vegetation. *J. Geophys. Res.*(submitted).

McDonald, J.E., 1960: Direct absorption of solar radiation by atmospheric water vapor. *J. Meteor.*, 17, 319-328.

McNider, R.T., 1981: Investigation of the impact of topographic circulations on the transport and dispersion of air pollutants. Ph.D. dissertation, University of Virginia, Charlottesville, VA 22903.

Orlanski, I., 1976: A simple boundary condition for unbounded hyperbolic flows. *J. Comput. Phys.*, 21, 251-269.

Perkey, D.J. and C.W. Kreitzberg, 1976: A time-dependent lateral boundary scheme for limited-area primitive equation models. *Mon. Wea. Rev.*, **104**, 744-755.

Rodgers, C.D., 1967: The use of emissivity in atmospheric radiation calculations. *Quart. J. Roy. Meteor. Soc.*, **93**, 43-54.

Sasamori, T., 1972: A linear harmonic analysis of atmospheric motion with radiative dissipation. *J. Meteor. Soc. of Japan*, **50**, 505-518.

Stephens, G.L., 1977: The transfer or radiation in cloudy atmosphere. Ph.D. Thesis. Meteorology Department, University of Melbourne.

Stephens, G.L., 1978a: Radiation profiles in extended water clouds. Webster Theory. *J. Atmos. Sci.*, **35**, 2111-2122.

Tremback, C.J. and R. Kessler, 1985: A surface temperature and moisture parameterization for use in mesoscale numerical models. Preprints, 7th Conference on Numerical Weather Prediction, 17-20 June 1985, Montreal, Canada, AMS.

Tremback, C.J., J. Powell, W.R. Cotton, and R.A. Pielke, 1987: The forward in time upstream advection scheme: Extension to higher orders. *Mon. Wea. Rev.*, **115**, 540-555.

Tremback, C.J., G.J. Tripoli, and W.R. Cotton, 1985: A regional scale atmospheric numerical model including explicit moist physics and a hydrostatic time-split scheme. Preprints, 7th Conference on Numerical Weather Prediction, June 17-20, 1985, Montreal, Quebec, AMS.

Tripoli, G.J. and W.R. Cotton, 1980: A numerical investigation of several factors contributing to the observed variable intensity of deep convection over South Florida. *J. Appl. Meteor.*, **19**, 1037-1063.

Tripoli, G.J., and W.R. Cotton, 1982: The Colorado State University three-dimensional cloud/mesoscale model - 1982. Part I: General theoretical framework and sensitivity experiments. *J. de Rech. Atmos.*, **16**, 185-220.

Yamamoto, G., 1962: Direct absorption of solar radiation by atmospheric water vapor carbon dioxide and molecular oxygen. *J. Atmos. Sci.*, **19**, 182-188.

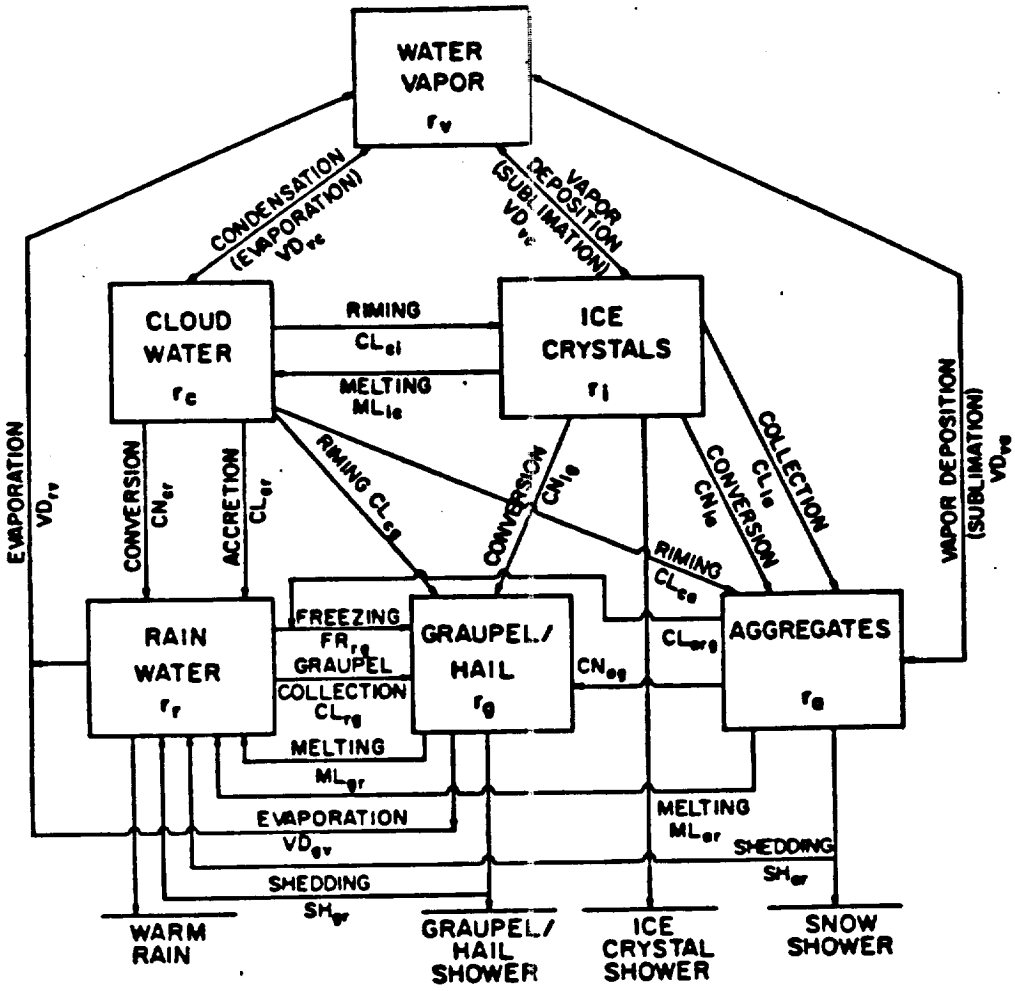

Figure 1: Flow diagram.

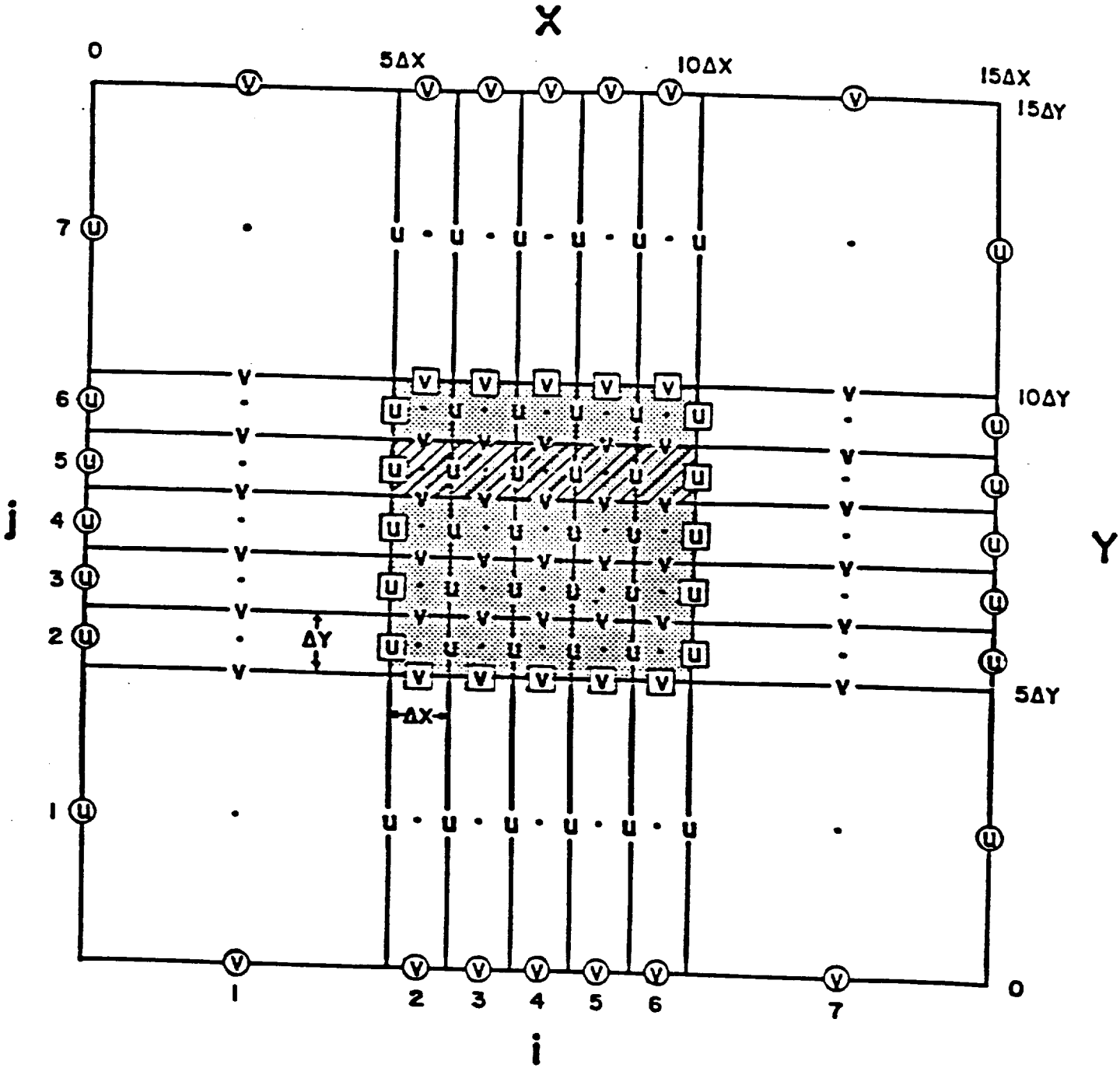

Figure 2: Mesoscale Compensation Region